DOI: http://dx.doi.org/10.26483/ijarcs.v15i2.7069

ISSN No. 0976-5697

Volume 15, No. 2, March-April 2024

International Journal of Advanced Research in Computer Science

RESEARCH PAPER

Available Online at www.ijarcs.info

FRACTAL FRACTIONAL MODEL OF RADIATIVE HEAT AND MASS TRANSFER CHARACTERISTICS OF TIME DEPENDENT FLOW WITH VARIABLE VISCOSITY, INDUCED MAGNETIC FIELD, DUFOUR AND SORET EFFECTS: AN ENTROPY GENERATION

Kidney Josiah Chillingo
The Local Government Training Institute,
Dodoma, Tanzania

Jumanne Mng'ang'a
The Local Government Training Institute,
Dodoma, Tanzania

Angelika M. Kayanda
The Local Government Training Institute,
Dodoma, Tanzania

Abstract: In this article, the Caputo Fabrizio fractal fractional order derivatives operator with an exponential kernel was employed to examine the radiative heat and mass transfer characteristics of time dependent flow with variable fluid viscosity, induced magnetic field, Soret and Dufour effects. The local mathematical model for the flow problem is formulated by take into account the impacts of thermal radiation, heat source, and viscous dissipation. The governing equations in-terms of fractal fractional model with an exponential kernel were solved numerically using finite difference method. The influence of flow variables such as induced magnetic field, concentration field, entropy rate, thermal field, and velocity field profiles against the pertinent parameters are discussed through graphs. Increase the values of magnetic Prandtl number results to rises of induced magnetic field. Higher Dufour number significantly grows the thermal field. The fractal fractional parameters enhance the velocity field, thermal field, Bejan number, entropy rate, concentration field and induced magnetic field profiles. The velocity field profiles recede with higher values of fluid variable viscosity parameter whereas the thermal field and induced magnetic field has an opposite effect. Larger Soret number amplifies the concentration field. Increase of Brinkman number, thermal radiation parameter, and magnetic Prandtl number intensifies the entropy generation rate. Increases of Brinkman number, magnetic Prandtl number, Soret number and Dufour number leads to a decrease of Bejan number whereas Bejan number rises with an increase of thermal radiation parameter and heat source.

Keywords: Fractional order; Variable viscosity; Induced magnetic field; Dufour-Soret; Finite difference method; entropy generation

INTRODUCTION

In various energy engineering and transformation operations, such as cancer therapy, nuclear power plants, and aircraft gadgets, radiation heat creation is crucial for the structure and development of equipment. The difficulties or challenges of creating industrial processes employing the radiation effect are investigated by many scientists and engineers through a variety of experiments and theoretical analyses. Li et al. [1] studied the influence of chemical reaction and properties of unstable MHD that dissipate energy in the presence of an activation energy in compressed Casson fluid flow through a horizontal channel. Chu et al. [2] analyzed the stretched nanomaterial containing Arrhenius catalysts has a double diffusion impact on the bio-convective magnetized flow of tangent hyperbolic liquid. Liu et al. [3] explored numerically bio- convective analysis of rate type nanofluid affected by Nield thermal restrictions and distinctive slip features. Li et al. [4] presented Utilizing stagnation point flow to generate entropy, the Carreau nanofluid's bioconvection effect uses the Cattaneo-Christov heat flux. Hussain et al. [5] investigated gyrotactic microorganism dynamics for chemically reactive magnetized 3D Sutterby nanofluid flow with non-uniform heat sink-source characteristics. Hussain et al. [6] studied Williamson nanofluid convectively heated radiative flow is impacted by ferromagnetic nanoparticles. Zafar et al. [7] analyzed gyrotactic microorganisms for the simulating Prandtl Nanofluid in mixed convective activation energy flow. Waqas et al. [8] examined analytically the shape factor effects on the flow of a dissipative SW/MWCNT-nanofluid coating from a stretching wall to a porous medium. Rathore and Sandeep [9] performed mono- and trihybrid nanofluids under solar thermal energy in the evacuated thermal collector tube. Chu et al. [10] studied the Hybrid nanofluid's thermal impact is caused by a porous surface with thermo-diffusion properties that is inclined and oscillatory. Abbas et al. [11] analyzed comparative study of produced MHD radiative Sutterby fluid flow in an elastic stretching cylinder or sheet in the presence of fluctuating thermal radiation. Wang et al. [12] investigated impacts of solar radiation and chemical reactivity on the Buongiorno model's electromagnetic Maxwell nanofluid flow.

Recently, Babu et al. [13] studied viscous thermophoretic fluid that is chemically reactive and has a changeable thermal conductivity is flowing across a wedge. Kheder et al. [14] presented comparative analysis of the entropy generation for a general fluidin a sloped channel from the viewpoints of classical and non-Fourier's law. Sajid et al. [15] analyzed Tri-hybridity nanofluids flowing across a wedge with convective boundary restrictions and activation energy have an impact on endothermic and exothermic chemical processes. Nazeer et al. [16]

investigated the momentum and thermal transfer in the thermally heated square conduit using MHD nanofluid. ur Rahman et al. [17] studied an assessment of the effects of activation energy on MHD bioconvective flow of nanofluids. Maaitah et al. [18] presented an analysis of the viscous dissipation of Williamson fluid through a saturated porous plate that is horizontal and has a constant wall temperature. Kodi et al. [19] discussed Hall current, thermal radiation, and Soret effects in the unsteady magnetohydrodynamic flow of Jeffrey fluid over porous medium. Ali et al. [20] discussed the blood circulation, respiratory system, and Darcy Forchheimer flow of ternary hybrid nanofluid. Mahesh et al. [21] analyzed effects of radiation, Stefan blowing, and chemical reaction on the pair stress fluid flow in the stretching surface under an angled magnetic field. Sowmiya and Kumar [22] explored impacts of activation energy in porous media with MHD Maxwell nanofluid flow across a stretching cylinder with microorganisms. Sharma et al. [23] investigated numerically the radiative MHD using power-law fluid flow of blood through a curved artery with the Hall effect. Basit et al. [24] discussed an exponentially permeable stretching surface is used in the numerical modeling of the bioconvective Casson nanofluid. Hobiny et al. [25] analyzed numerically the viscosity dissipation in ferromagnetic Carreau fluid flow. Reddy et al. [26] investigated the influence of thermal radiation on MHD flow with non-linearly stretching sheet. The system's inability to fully utilize the energy it has available is known as its entropy. The key contributors to a system's increasing entropy include irreversible mass, heat, and fluid transfers, as well as fluid friction. The overall entropy of the system is the product of these three elements. The importance of irreversible elementsrelated to friction, heat transport, and other imperfect processes within a system is highlighted by entropy generation. Bhatti et al. [27] investigated the influence of an entropy generation and the nonlinear heat radiation on a porous shrinking sheet-based non-Newtonian nanofluid. Sudarsana Reddy and Sreedevi [28] studied in a square cavity with thermal radiation, a magnetic hybrid nanofluid is being studied for entropy formation and heat transfer. Sahoo and Nandkeolyar [29] analyzed the impacts of thermal radiation on a mixed convective flow of a Casson nanofluid with Hall current and dissipative heat transfer. Lopez et al. [30] discussed influence of nonlinear thermal radiation, and convective-radiative boundary conditions in MHD nanofluid flowin a vertical microchannel with slip flow. Reddy [31] analyzed biomedical features of flow of a hybrid nanofluid with the nonlinear thermal radiation and a non-uniform heat source/sink. Khan et al. [32] studied entropy production minimization is used to account for nonlinear radiative heat flux in convective nanomaterial flow. Salawu and Ogunseye [33] investigated an entropy production in a Powell-Eyring chemical reaction involving a nanofluid with varying conductivity and electric fields. Ullah et al.
[34] studied numerically the finite difference approach for entropy generation and heat transfer study in power-law fluid flow. Muhammad et al. [35] analyzed the influence ofsecond order slip and an entropy creation were generated by the magnetohydrodynamics radiation of nanomaterial and viscous flow in the curved surface. Shah et al. [36] investigated influence of the radiative and chemical reacting on MHD Casson Nanofluid Flow over past nonlinearly stretched surfaces with activation energy.
Khan et al. [37] studied numerically the MHD mixed convective radiative slip flow with varying fluid parameters and the presence of an entropy generation. Khan et al. [38] studied the main characteristics of the Dufour and Soret effect in the radiative MHD flow of a viscous fluid via a rotating cone with entropy generation. Khan et al. [39]analyzed the thermal analysis of Darcy-Forchheimer nanoparticles exposed to entropy generation in radiative flow. Hayat et al. [40] analyzed numerically using finitedifference method for Casson fluid flow with diffusion-thermal and thermo diffusion effects. Subramanyam Reddy et al. [41] presented an entropy generation in a vertical channel with pulsatile flow of Jeffrey hybrid nanofluid. Dadheech et al. [42] studied an entropy generation analysis of two separate fluids through a porous medium during radiative inclined MHD slip flow with heat sink/source. Khan et al. [43] analyzed anentropy production in a chemically reactive flow of a Reiner-Rivlin liquid carrying tiny particles is considered in the presence of thermal radiation. Li et al. [44] analyze the heat and mass transfer in a radiative, time-dependent flow with chemical reaction,ohmic heating, and viscous dissipation. Li et al. [45] studied the Sutterby nanomaterial flow optimized for entropy in a porous medium. Hussain et al. [46] studied numerically the Darcy-Forchheimer flow in the vertical flat plate with uneven heat source/sink of cross nanofluids. Murtaza et al. [47] studied the use of finite difference on casson fluidin a micro channel by employing the fractal fractional order operator.
In 1873, the Dufour effect, or thermal flux caused by a concentration gradient, was identified by Charles L. Dufour. It is known as the diffusion-thermo effect. However, Soret was aware that a temperature differential may cause a mass flux. Here is an illustration of the thermal-diffusion effect. When the flow regime has large density differences, Dufour and Soret impacts become important. the thermal radiation, Du- four, and Soret impacts on magnetohydrodynamic flows can be seen in engineering applications such as heat insulation, geothermal systems, MHD generators, and drying technology. Ahmed [48] investigated the diffusion-thermo and MHD radiating flowwith thermal diffusion. Mouli et al. [49] discussed the effects of Soret and Dufour on Sutterby fluid after a stretching sheet using spectral relaxation approach. In the presence of thermal buoyancy, viscous dissipation, and unstable heat and mass transfer flow, the positive and negative effects of the Soret and Dufour are examined by Falodun et al. [50]. Using a heat sink, a porous medium, and double diffusive convection, cross diffusive effects on a Casson fluid across a Riga plate are studied by Asogwa et al. [51]. Prasad et al. [52] presented the impact of double diffusivity on mixed convection Casson fluid passing a wavering inclined plate in the porous Darcian medium. Akram et al. [53] examined the partial slip on Eyring-Powell nanofluids' double-diffusion convection under the influence of peristaltic propulsion and an angled magnetic field from a theoretical perspective. Negi et al. [54]

discussed the Stefan blowing impact on copper-water nanofluid flow over a stretching surface in theCattaneo-Christov double-diffusion model. Mondal and Mahapatra [55] explored the MHD nanofluid convection and entropy formation in a trapezoidal cavity with the double-diffusive. Noon and Haddad [56] analyzed the rotating double-diffusive convection's stability under varying gravity conditions and with reaction effects. Bouachir et al. [57] investigated double-diffusive convection with an influence of Soret and Dufour in a vertical brinkman porous enclosure. Vijay and Sharma [58] discussed the influence of Soret and Dufour in MHD hybrid nanofluid flow across a rotating disk. Mishra et al. [59] studied the blood flow via a stenosed artery with varying viscosity under the impacts of Soret and Dufour.

Induced magnetic field on MHD flow of mass and heat transfer continues to be of interest to researchers due to its various range of practical applications in engineering, science, and technology. Ramzan et al. [60] studied the computational analysis of the Cattaneo-Christov heat flux and the impacts of induced magnetic field in the flow of nanofluid along a curved surface. Mng'ang'a et al. [61] explored the effects of a chemical reaction and an induced magnetic field on an MHD surface-driven flow. Dolui et al. [62] studied the combined effects of thermal radiation and induced magnetic field together have an impact on the flow of a ternary hybrid nanofluid via an angled catheterized artery with multiple stenosis . Khan et al. [63] discussed the Water-based graphene-oxide flow at the point of stagnation over a stretching/shrinking sheet in an induced magnetic field with heterogeneous and homogeneous chemical reaction. Akram et al. [64] studied numerically Ellis nanofluid undergoes twofold diffusion convection during peristaltic pumping as a result of an induced magnetic field in a non-uniform channel. Mng'ang'a [65] investigated the effects of Newtonian cooling, chemical reaction, induced magnetic field, and Joule heating on MHD generalized Couette flow. Akram et al. [66] presented the effects of hybrid double-diffusivity convection and an induced magnetic field on the peristaltic waves of Oldroyd 4-constant nanofluids in a non-uniform channel. Akram et al. [67] investigated the hyperbolic tangent nanofluid flowing in a non-uniform channel with an induced magnetic field under double-diffusiveconvection. Mng'ang'a [68] studied the influence of Ohmic heating, induced magnetic field, and Newtonian heating on Jeffrey nanofluid Couette flow with convective coolingbetween the horizontal surfaces. Singh et al. [69] investigated the effects of the Hall current and induced magnetic field on transient MHD nanofluid flow between two vertically alternate magnetized surfaces. Mahato et al. [70] studied unsteady radiative hydromagnetic mixed convection Casson fluid flow with Soret effect, induced magnetic field, chemical reaction, and convective boundary conditions approaching a stagnation point. Alam et al. [71] discovered the impacts of induced magnetic field on mixed convection flow of vertical plate with constant heat, and mass fluxes.

From the comprehensive literature mentioned above includes multiple investigations on the MHD flow of various fluids with or without induced magnetic fields in the flow. Considering the importance of combined effects of heat and mass transfer with induced magnetic field, variable fluid viscosity, and thermal radiation on different field of technology, science, and engineering. No such study has been reported on the numerical analysis of the Caputo-Fabrizio fractal-fractional model of radiative heat and mass transfer characteristic of time flow dependent flow with exponential kernel. The main novelty of the present study is to apply the Caputo-Fabrizio fractal fractional order derivatives operator with exponential kernel on the combined effects of variable fluid viscosity, induced magnetic field, Dufour, and Soret effects on radiative time dependent flow. In addition the viscous dissipation, thermal radiation, entropy generation, and heat source has also been considered. The non-linear PDEs of the governing equation were solved numerically using finite difference method. The effects of embedded parameters on the flow variables are given through graphs and discussed in detail.

MATHEMATICAL MODEL FORMULATION WITH FRACTAL FRACTIONAL OPERATOR

Consider bi-dimensional reactive unsteady hydromagnetic, laminar flow, viscous liquid flow and electrically conducting fluid in the flat plate with an induced magnetic field $\vec{B}_y$, a uniform constant suction $u' = u_o$ across an infinite flat plate. The Fractal fractional model of radiative heta ans mass transfer consider the impacts of thermal radiation, heat source, magnetic fields and viscous dissipation. no external forces including gravity is taken into account in the flow. The magnetic field vector is $(\vec{B}_y, \vec{B}_0)$ such that a constant magnetic field B_0 applied perpendicular to the plate as shown in the figure 1.

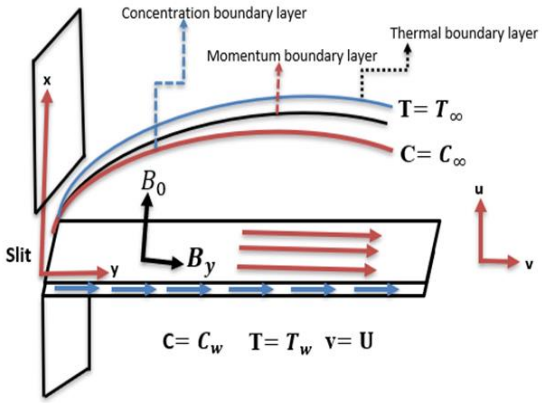

Fig 1: Geometry of the problem.

The governing equations such as continuity , momentum , energy, concentration, and magnetic induction equations of the present physical system are as follow[26,72,74]:-

$$\frac{\partial u\prime}{\partial x\prime} = 0 \Rightarrow u' = -u_0 \tag{1}$$

$$\frac{\partial v\prime}{\partial t\prime} = u_0 \frac{\partial v\prime}{\partial x\prime} + \frac{\mu_e B_0}{\rho}\frac{\partial B\prime_y}{\partial x\prime} + \frac{\partial}{\partial x\prime}\left(\mu(T')\frac{\partial v\prime}{\partial x\prime}\right) \tag{2}$$

$$\begin{aligned}\frac{\partial T\prime}{\partial t\prime} = \; & u_0 \frac{\partial T\prime}{\partial x\prime} + \frac{16\sigma T_\infty'^3}{3k(\rho C_p)}\frac{\partial^2 T\prime}{\partial x\prime^2} + \frac{k}{\rho C_p}\left(\frac{\partial^2 T\prime}{\partial x\prime^2}\right) + \frac{1}{\rho C_p}\left(\frac{\partial B\prime_y}{\partial x\prime}\right)^2 \\ & + \frac{K_t D_m}{C_p C_s}\frac{\partial^2 C\prime}{\partial x\prime^2} + \frac{W(T\prime - T_\infty)}{\rho C_p} + \frac{\mu(T\prime)}{\rho C_p}\left(\frac{\partial v\prime}{\partial x\prime}\right)^2\end{aligned} \tag{3}$$

$$\frac{\partial C\prime}{\partial t\prime} = u_0 \frac{\partial C\prime}{\partial x\prime} + \frac{D_m K_t}{T_m}\frac{\partial^2 T\prime}{\partial x\prime^2} + D_m \frac{\partial^2 C\prime}{\partial x\prime^2} + K_r(C_\infty - C') \tag{4}$$

$$\frac{\partial B\prime_y}{\partial t\prime} = \frac{\partial B\prime_y}{\partial x\prime}u_0 + \frac{1}{\mu(T\prime)\sigma}\left(\frac{\partial^2 B\prime_y}{\partial x\prime^2}\right) + \frac{\partial v\prime}{\partial x\prime}B_0 \tag{5}$$

Initial and boundary conditions are as follows[26,72,74] :-
$$\begin{cases} v' = 0, C' = C_\infty, B'_y = 0, T' = T_\infty & \text{at} \quad t' = 0 \\ v' = U, C' = C_w, B'_y = B_0, T' = T_w & \text{at} \quad x' = 0 \\ v' = 0, C' = C_\infty, B'_y = 0, T' = T_\infty & \text{as} \quad x' \to \infty \end{cases} \tag{6}$$

In this study the fluid viscosity is assumed to vary exponentially with temperature of the fluid following [73] is given as follows:-

$$\mu(T) = \mu_0 e^{\alpha(T_\infty - T\prime)} \tag{7}$$

To non-dimensionalize the governing equations, We use the following dimensionless varaibles or quantities for the present magnetohydrodynamic problem:-

$$\begin{aligned} & B^* = \sqrt{\frac{\mu_e}{\rho}}\frac{L}{\nu}B'_y, \quad V = \frac{L}{\nu}v', \qquad C' = C_\infty + \phi(C_w - C_\infty), \\ & T' = T_\infty + \theta(T_w - T_\infty), \qquad t' = \frac{h^2\tau\prime}{\nu}, \quad x' = L'\eta' \end{aligned} \tag{8}$$

Utilizing the dimensionless quantities or variables defined in Eq.(8); The governing equations defined in Eqs.(2), (4), (5) and (3), in dimensionless form are as follows:-

$$\frac{\partial V}{\partial \tau\prime} = S\frac{\partial V}{\partial \eta\prime} + M\frac{\partial B_y^*}{\partial \eta\prime} + e^{\varepsilon\theta}\frac{\partial^2 V}{\partial \eta\prime^2} + \varepsilon\frac{\partial V}{\partial \eta}\frac{\partial \theta}{\eta} \tag{9}$$

$$\frac{\partial \theta}{\partial \tau\prime} = S\frac{\partial \theta}{\partial \eta'} + Q\theta + e^{\varepsilon\theta}Ec\left(\frac{\partial V}{\partial \eta'}\right)^2 + J\left(\frac{\partial B^*}{\partial \eta'}\right)^2 Du\frac{\partial^2 \phi}{\partial \eta'^2} + \frac{1}{Pr}\left(\frac{4}{3} + R\right)\frac{\partial^2 \theta}{\partial \eta\prime^2} \tag{10}$$

$$\frac{\partial \phi}{\partial \tau\prime} = S\frac{\partial \phi}{\partial \eta\prime} + Sr\frac{\partial^2 \theta^*}{\partial \eta\prime^2} + \frac{1}{Sc}\frac{\partial^2 \phi}{\partial \eta\prime^2} \tag{11}$$

$$\frac{\partial B^*}{\partial \tau\prime} = S\frac{\partial B^*}{\partial \eta\prime} + \frac{1}{e^{\varepsilon\theta}Pr_m}\left(\frac{\partial^2 B^*}{\partial \eta\prime^2}\right) - \frac{\partial V}{\partial \eta\prime} \tag{12}$$

where by J represent Joule heating parameter, Gr represent thermal Grashof number, R represent thermal radiation parameter, Sr represent Soret number, M represent magnetic parameter, S represent suction parameter, Sc represent Schmidt number, Pr represent Prandtl number, Du represent Dufour number, Q represent heat source parameter, Pr_m represent magnetic Prandtl number, Gc represent mass Grashof number, and Ec represent Eckert number which are defined mathematical as follows:-

$$\begin{aligned} & Ec = \frac{U'^2}{c_p(T_w - T_\infty)}, Gr = \frac{g\beta_*^t h^2(T_w - T_\infty)}{\nu U'}, \\ & S = \frac{u_0}{U\prime}, Sc = \frac{\nu}{D}, R_d = \frac{4\sigma T_\infty'^3 \nu}{k\rho C_p h^2}, Sr = \frac{D_m K_t(T_w - T_\infty)}{T_m(C_w - C_\infty)\nu}, Pr = \frac{\mu c_p \nu}{k}, M = \frac{B_0\mu_e h^2}{U\prime\nu\rho}, Du = \frac{K_t D_m(C_w - C_\infty)}{\nu C_p C_s(T_w - T_\infty)}, \\ & Q = \frac{h^2 W}{\nu\rho c_p}, J = \frac{B_0^2}{\rho C_p \nu(T_w - T_\infty)} \\ & Gc = \frac{g\beta_*^c h^2(C_w - C_\infty)}{\nu U\prime}, Pr_m = \mu_e\sigma\nu \end{aligned} \tag{13}$$

initial and boundary conditions are as follows:-

$$\begin{cases} V=0,\phi=0,B=0,\theta=0, & \text{at} \quad \tau=0 \\ V=1,\phi=1,B=1,\theta=1, & \text{at} \quad \eta=0 \\ V=0,\phi=0,B=0,\theta=0, & \text{as} \quad \eta\to\infty \end{cases} \tag{14}$$

The Caputo-Fabrizio with non singular exponential kernel is given by

$$^{C}D_t^{\alpha}f(x,t)=\frac{M(\alpha)}{1-\alpha}\int_0^t \frac{\partial f(x,t)}{\partial\tau}exp\left(-\frac{\alpha(t-\tau)}{1-\alpha}\right)d\tau$$
$$0<\alpha<1 \tag{15}$$

where by $M(\alpha)$ represent normalization function and $\frac{M(\alpha)}{1-\alpha}exp\left(-\frac{\alpha(t-\tau)}{1-\alpha}\right)$ represent non-singular exponential kernel.

The exponential decay kernel of the fractal-fractional derivative of order α in the Riemann-Liouville sense is given as follows[47]:-

$$^{FF}D_x^{\alpha,\beta}f(x)=\left(\frac{M(\alpha)}{1-\alpha}\right)x^{\beta}\int_0^x f(\xi)exp\left(-\frac{\alpha(x-\xi)}{1-\alpha}\right)d\xi$$
$0<\alpha,\beta\leqslant 1$ (16)

where $M(0)=M(1)=1$.

The classical governing equations given in (9), (10), (11) and (12) are transformed into the governing equations of the Caputo-Fabrizio fractal-fractional operator with exponential kernel take the following form[47]:-

$$^{FF}D_{\tau'}^{\alpha,\beta}V=S\frac{\partial V}{\partial\eta'}+M\frac{\partial B_y^*}{\partial\eta'}+e^{\varepsilon\theta}\frac{\partial^2 V}{\partial\eta'^2}+\varepsilon\frac{\partial V}{\partial\eta}\frac{\partial\theta}{\eta} \tag{17}$$

$$^{FF}D_{\tau'}^{\alpha,\beta}\theta=S\frac{\partial\theta}{\partial\eta'}+Q\theta+e^{\varepsilon\theta}Ec\left(\frac{\partial V}{\partial\eta'}\right)^2+J\left(\frac{\partial B^*}{\partial\eta'}\right)^2Du\frac{\partial^2\phi}{\partial\eta'^2}+\frac{1}{Pr}\left(\frac{4}{3}+R\right)\frac{\partial^2\theta}{\partial\eta'^2} \tag{18}$$

$$^{FF}D_{\tau'}^{\alpha,\beta}\phi=S\frac{\partial\phi}{\partial\eta'}+Sr\frac{\partial^2\theta^*}{\partial\eta'^2}+\frac{1}{Sc}\frac{\partial^2\phi}{\partial\eta'^2} \tag{19}$$

$$^{FF}D_{\tau'}^{\alpha,\beta}B^*=S\frac{\partial B^*}{\partial\eta'}+\frac{1}{e^{\varepsilon\theta}Pr_m}\left(\frac{\partial^2 B^*}{\partial\eta'^2}\right)-\frac{\partial V}{\partial\eta'} \tag{20}$$

Here $^{FF}D_{\tau'}^{\alpha,\beta}$ represent the fractal fractional operator with an exponential kernel following by

$$^{FF}D_{\tau}^{\alpha,\beta\Theta(\tau)}=\left(\frac{N(\alpha)}{1-\alpha}\right)\tau^{\beta}\int_0^{\tau}\Theta(\xi)exp\left(-\frac{\alpha(\tau-\xi)}{1-\alpha}\right)d\xi$$
$0<\alpha,\beta\leqslant 1.$ (21)

where $N(0)=N(1)=1$

ENTROPY GENERATION ANALYSIS

The reduction of energy resource waste is one of the key factors for scientists and researchers. It is essential to increase the effectiveness of current systems. This makes it possible to examine how entropy is produced in systems and contributes to the irreversibility of energy. the following definition of entropy generation

$$E_G{}'=\frac{1}{\sigma T_\infty}\left(\frac{\partial B}{\partial x'}\right)^2+\frac{k}{T_\infty}\left(1+\frac{16\sigma_S T_\infty'^3}{3kk_f}\right)\left(\frac{\partial T'}{\partial x'}\right)^2+\frac{\mu}{T_\infty}\left(\frac{\partial v'}{\partial x'}\right)^2+\frac{RD_m}{T_\infty}\frac{\partial T'}{\partial x'}+HT+\frac{RD_m}{C_\infty}\left(\frac{\partial C'}{\partial x'}\right) \tag{22}$$

But S_G can be defined as $S_G=\frac{E_G{}'T_\infty}{k(T_w-T_\infty)}$ (23)

Finally becomes

$$S_G=BrPrm\left(\frac{\partial B^*}{\partial\eta'}\right)^2+\alpha(1+Rd)\left(\frac{\partial\theta}{\partial\eta'}\right)^2+Q\theta+Sr\left(\frac{\partial\phi}{\partial\eta'}\right)+Br\left(\frac{\partial V}{\partial\eta'}\right)^2+Du\frac{\partial\theta}{\partial\eta'} \tag{24}$$

The Bejan number (Be) is defined as entropy generation due to the heat transfer over total entropy generation. we have

$$Be=\frac{\alpha(1+Rd)\left(\frac{\partial\theta}{\partial\eta'}\right)^2}{BrPrm\left(\frac{\partial B^*}{\partial\eta'}\right)^2+\alpha(1+Rd)\left(\frac{\partial\theta}{\partial\eta'}\right)^2+Br\left(\frac{\partial V}{\partial\eta'}\right)^2+Du\frac{\partial\theta}{\partial\eta'}+Q\theta+Sr\left(\frac{\partial\phi}{\partial\eta'}\right)} \tag{25}$$

NUMERICAL SOLUTION

The governing equations(17), (18), (19) and (20) are highly nonlinear coupled PDEs and the numerical solution doesn't found in the close forms, and thus are solved numerically by using finite difference method with an appropriate boundary conditions (14). The mesh size is fixed at $\Delta\eta = 0.025$ in $x-$direction and $\Delta\tau = 0.00112$ at time level has been used to all numerical simulation to ensure that there is stability and convergence. The absolute error for all grid nodes, that is the expression $|\varphi^{rn+1} - \varphi^{rn}| \leqslant 10^{-7}$ is considered as convergence criterion, where rn represent repetition number and φ represents $[V, \theta, \phi, B^*]^T$.

A discrete approximation to the Caputo-Fabrizio Fractal-Fractional derivatives operator can be obtained by using quadrature formula as follows[47]:-

$$ {}^{FF}D_{\tau'}^{\alpha,\beta}\,\Theta(\tau') = \left(\frac{N(\alpha)}{1-\alpha}\right)\frac{d}{d\tau^{\beta}}\int_0^{\tau}\Theta(\xi)exp\left(-\frac{\alpha(\tau'-\xi)}{1-\alpha}\right)d\xi, 0<\alpha,\beta\leqslant 1 \tag{26}$$

discretizing the above equation ,we have:-

$$ {}^{FF}D_{\tau'}^{\alpha,\beta}\,\Theta(\tau_k) = \left(\frac{N(\alpha)}{1-\alpha}\right)\beta{\tau_k}^{\beta-1}\sum_{j=1}^{n}\int_{(\mathrm{k}-1)\mathrm{j}}^{kj}\left(\frac{\Theta_i^{j+1}-\Theta_i^{j}}{\gamma}\right)\times exp\left(-\frac{\alpha(\tau'-\xi)}{1-\alpha}\right)d\xi \tag{27}$$

$$ {}^{FF}D_{\tau'}^{\alpha,\beta}\,\Theta(\tau_k) = \left(\frac{N(\alpha)}{1-\alpha}\right)\beta{\tau_k}^{\beta-1}\sum_{j=1}^{n}\left(\frac{\Theta_i^{j+1}-\Theta_i^{j}}{\gamma}\right)\times\int_{(\mathrm{k}-1)\mathrm{j}}^{kj} exp\left(-\frac{\alpha(\tau'-\xi)}{1-\alpha}\right)d\xi \tag{28}$$

which is equivalent to

$$ {}^{FF}D_{\tau_k}^{\alpha,\beta}\,\Theta(\tau,\eta') = \frac{N(\alpha)}{\alpha}\beta\tau_k^{\beta-1}\left\{\left(\frac{\Theta_i^{j+1}-\Theta_i^{j}}{\tau}\right)+\sum_{j=1}^{n}\left(\frac{\Theta_i^{j+1-n}-\Theta_i^{j-n}}{\tau}\right)\right\}\Delta_{j,n} \tag{29}$$

but $\Delta_{j,n} = erf\left\{\frac{\alpha j}{1-\alpha}(n-j)\right\} - erf\left\{\frac{\alpha j}{1-\alpha}(n-j+1)\right\}$

Similarly, other classical derivatives can be approximated as follows:-

$$\begin{aligned}&\frac{\partial\theta}{\partial\eta'} = \frac{\theta_j^n-\theta_{j-1}^n}{\Delta\eta'}, \frac{\partial\phi}{\partial\eta'} = \frac{\phi_j^n-\phi_{j-1}^n}{\Delta\eta'}, \theta=\theta_j^n, V=V_j^n, \frac{\partial V}{\partial\eta'} = \frac{V_j^n-V_{j-1}^n}{\Delta\eta'},\\ &,\frac{\partial^2\theta}{\partial\eta'^2} = \frac{\theta_{j-1}^n-2\theta_j^n+\theta_{j+1}^n}{(\Delta\eta')^2}, \phi=\phi_j^n, \frac{\partial^2\phi}{\partial\eta'^2} = \frac{\phi_{j-1}^n-2\phi_j^n+\phi_{j+1}^n}{(\Delta\eta')^2}, \quad \frac{\partial B}{\partial\eta} = \frac{B_j^n-B_{j-1}^n}{2\Delta\eta'}, B=B_j^n\\ &\frac{\partial^2 V}{\partial\eta'^2} = \frac{V_{j-1}^n-2V_j^n+V_{j+1}^n}{(\Delta\eta')^2}, \frac{\partial^2 B}{\partial\eta'^2} = \frac{B_{j-1}^n-2_j^{n+1}+B_{j+1}^n}{(\Delta\eta')^2}.\end{aligned} \tag{30}$$

Using equations (29) and (30) into equations (17), (18), (19) and (20), the finite difference corresponding to the fractal fractional governing equations are as follows:-

$$\frac{V_j^{n+1}-V_j^n}{\Delta\tau'} = \left(\begin{array}{l} S\left(\frac{V_j^n-V_{j-1}^n}{\Delta\eta'}\right)+M\left(\frac{B_j^n-B_{j-1}^n}{\Delta\eta'}\right)+e^{\varepsilon\theta_j^n}\left(\frac{V_{j-1}^n-2V_j^n+V_{j+1}^n}{(\Delta\eta')^2}\right)+\\ \varepsilon\left(\frac{v_j^n-v_{j-1}^n}{\Delta\eta'}\right)\left(\frac{\theta_j^n-\theta_{j-1}^n}{\Delta\eta'}\right)-\left(\frac{N(\alpha)}{\alpha}\beta\Delta\tau'^{\beta-1}\right)\times\\ \sum_{n=1}^{m}\left[\left(\frac{V_j^{n+1-m}-V_j^{n-m}}{\Delta\tau'}\right)\right]\times\\ \sum_{n=1}^{m}\left[\left(erf\left\{\frac{\alpha n}{1-\alpha}(m-n)\right\}-erf\left\{\frac{\alpha n}{1-\alpha}(m-n+1)\right\}\right)\right]\end{array}\right)\times$$

$$\left(\frac{N(\alpha)}{\alpha}\beta\Delta\tau'^{\beta-1}\left(erf\left\{\frac{\alpha n}{1-\alpha}(m-n)\right\}-erf\left\{\frac{\alpha n}{1-\alpha}(m-n+1)\right\}\right)\right)^{-1} \tag{31}$$

$$\frac{\theta_j^{n+1}-\theta_j^n}{\Delta\tau'} = \left(\begin{array}{l} S\left(\frac{\theta_j^n-\theta_{j-1}^n}{\Delta\eta'}\right)+\frac{1}{Pr}\left(\frac{4}{3}+Rd\right)\left(\frac{\theta_{j-1}^n-2\theta_j^n+\theta_{j+1}^n}{(\Delta\eta')^2}\right)+\\ e^{\varepsilon\theta_j^n}Ec\left(\frac{V_j^n-V_{j-1}^n}{\Delta\eta'}\right)^2+Du\left(\frac{\phi_{j-1}^n-2\phi_j^n+\phi_{j+1}^n}{(\Delta\eta')^2}\right)+Q\theta_j^n+\\ J\left(\frac{B_j^n-B_{j-1}^n}{\Delta\eta'}\right)^2-\left(\frac{N(\alpha)}{\alpha}\beta\Delta\tau'^{\beta-1}\right)\times\sum_{n=1}^{m}\left[\left(\frac{\theta_j^{n+1-m}-\theta_j^{n-m}}{\Delta\tau'}\right)\right]\times\\ \sum_{n=1}^{m}\left[erf\left\{\frac{\alpha n}{1-\alpha}(m-n)\right\}-erf\left\{\frac{\alpha n}{1-\alpha}(m-n+1)\right\}\right]\end{array}\right)\times \tag{32}$$

$$\left(\frac{N(\alpha)}{\alpha}\beta\Delta\tau'^{\beta-1}\left(erf\left\{\frac{\alpha n}{1-\alpha}(m-n)\right\}-erf\left\{\frac{\alpha n}{1-\alpha}(m-n+1)\right\}\right)\right)^{-1}$$

$$\frac{\phi_j^{n+1}-\phi_j^n}{\Delta\tau'} = \left(\begin{array}{l} S\left(\frac{\phi_j^n-\phi_{j-1}^n}{\Delta\eta'}\right)+\frac{1}{Sc}\left(\frac{\phi_{j-1}^n-2\phi_j^n+\phi_{j+1}^n}{(\Delta\eta')^2}\right)+Sr\left(\frac{\theta_{j-1}^n-2\theta_j^n+\theta_{j+1}^n}{(\Delta\eta')^2}\right)- \\ \left(\frac{N(\alpha)}{\alpha}\beta\Delta\tau'^{\beta-1}\right)\times\sum_{n=1}^{m}\left[\left(\frac{\phi_j^{n+1-m}-\phi_j^{n-m}}{\Delta\tau'}\right)\right]\times \\ \sum_{n=1}^{m}\left[erf\left\{\frac{\alpha n}{1-\alpha}(m-n)\right\}-erf\left\{\frac{\alpha n}{1-\alpha}(m-n+1)\right\}\right] \end{array} \right)\times \tag{33}$$

$$\left(\frac{N(\alpha)}{\alpha}\beta\Delta\tau'^{\beta-1}\left(erf\left\{\frac{\alpha n}{1-\alpha}(m-n)\right\}-erf\left\{\frac{\alpha n}{1-\alpha}(m-n+1)\right\}\right)\right)^{-1}$$

$$\frac{B_j^{n+1}-B_j^n}{\Delta\tau'} = \left(\begin{array}{l} S\left(\frac{B_j^n-B_{j-1}^n}{2\Delta\eta'}\right)-\left(\frac{V_j^n-V_{j-1}^n}{2\Delta\eta'}\right)+\frac{1}{e^{\varepsilon\theta_j^n}Pr_m}\left(\frac{B_{j-1}^n-2_j^n+B_{j+1}^n}{(\Delta\eta')^2}\right)- \\ \left(\frac{N(\alpha)}{\alpha}\beta\Delta\tau'^{\beta-1}\right)\times\sum_{n=1}^{m}\left[\left(\frac{B_j^{n+1-m}-B_j^{n-m}}{\Delta\tau'}\right)\right]\times \\ \sum_{n=1}^{m}\left[erf\left\{\frac{\alpha n}{1-\alpha}(m-n)\right\}-erf\left\{\frac{\alpha n}{1-\alpha}(m-n+1)\right\}\right] \end{array} \right)\times \tag{34}$$

$$\left(\frac{N(\alpha)}{\alpha}\beta\Delta\tau'^{\beta-1}\left(erf\left\{\frac{\alpha n}{1-\alpha}(m-n)\right\}-erf\left\{\frac{\alpha n}{1-\alpha}(m-n+1)\right\}\right)\right)^{-1}$$

The entropy rate in finite difference form become:-

$$\begin{aligned} S_G = \; & BrPrm\left(\frac{B_j^n-B_{j-1}^n}{\Delta\eta'}\right)^2+\alpha(1+Rd)\left(\frac{\theta_j^n-\theta_{j-1}^n}{\Delta\eta'}\right)^2+Br\left(\frac{V_j^n-V_{j-1}^n}{\Delta\eta'}\right)^2+ \\ & Du\left(\frac{\theta_j^n-\theta_{j-1}^n}{\Delta\eta'}\right)+Q\theta+Sr\left(\frac{\phi_j^n-\phi_{j-1}^n}{\Delta\eta'}\right) \end{aligned} \tag{35}$$

Bejan number in finite difference form becomes:-

$$Be = \frac{\alpha(1+Rd)\left(\frac{\theta_j^n-\theta_{j-1}^n}{\Delta\eta'}\right)^2}{BrPrm\left(\frac{B_j^n-B_{j-1}^n}{\Delta\eta'}\right)^2+\alpha(1+Rd)\left(\frac{\theta_j^n-\theta_{j-1}^n}{\Delta\eta'}\right)^2+Br\left(\frac{V_j^n-V_{j-1}^n}{\Delta\eta'}\right)^2+Du\left(\frac{\theta_j^n-\theta_{j-1}^n}{\Delta\eta'}\right)+Q\theta+Sr\left(\frac{\phi_j^n-\phi_{j-1}^n}{\Delta\eta'}\right)} \tag{36}$$

with initial and boundary conditions as follows:-

$$\begin{cases} V(0,n)=0,\phi(0,n)=0,B(0,n)=0,\theta(0,n)=0, & \text{at} \quad j=0 \\ V(j,0)=1,\phi(j,0)=1,B(j,0)=1,\theta(j,0)=1, & \text{at} \quad n=0 \\ V(j,n)=0,\phi(j,n)=0,B(j,n)=0,\theta(j,n)=0, & \text{as} \quad \forall j,n \end{cases} \tag{37}$$

RESULTS AND DISCUSSION

In this study, the fractal fractional order derivatives operator is utilized on the MHD fluid flow analysis of mass and heat transfer characteristic in radiative time dependent with variable viscosity, induced magnetic field, chemical reaction, thermo-diffusion and diffusion-thermo effects with an entropy generation have been investigated by incorporating the impact of thermal radiation, viscous dissipation and heat source. In order to get the physical insight, the effects of various key embedded parameters on the flow field profiles are scrutinized using graphical representation and the comparison of Velocity field profiles of fractal-fractional, fractional, fractal, and classical order models is presented through graph.

Figure 2 shows the Comparison of the Velocity field profiles of fractal-fractional, fractional, fractal, and classical order models against η for different values of fractal-fractional parameters α and β. From the graph, it can be seen that the velocity field profiles significantly grows. Physically, for higher values of fractal fractional parameter results to an increase of velocity field due to the fact that fractal fractional parameter has larger memory effects which cause the lower momentum boundary layer. From the graphs the fractal parameter β has great momentum boundary layer compered to fractional order operator α.

In comparison to fractional order and classical model, fractal-fractional has a strong memory effect. The fractal-fractional model has these characteristics because of the fractal parameter, which is absent fractional and classical models.The fractal-fractional model is handier and more realist to the real world phenomena due to the higher memory effect.

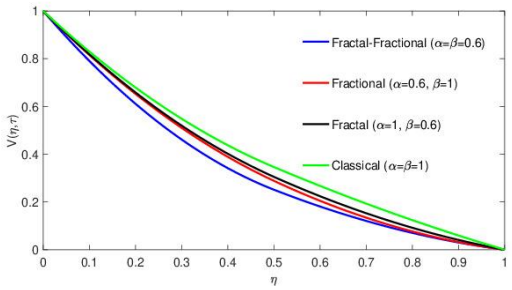

Fig 2: Comparison of the Velocity field ($V(\eta,\tau)$) of fractal-fractional, fractional, fractal,classical order models

Figure 3 presents the influence magnetic parameter (M) of the velocity profiles. Graphically, it's noted that the velocity profiles drops as the values of the magnetic

parameter rises. As expected, physically increasing the values of magnetic parameters causes slowly or resist the motion of the fluid. Since the magnetic field is perpendicular applied in the direction of the flow and thus reduce the velocity boundary layer thickness which cause the velocity profiles to decrease.

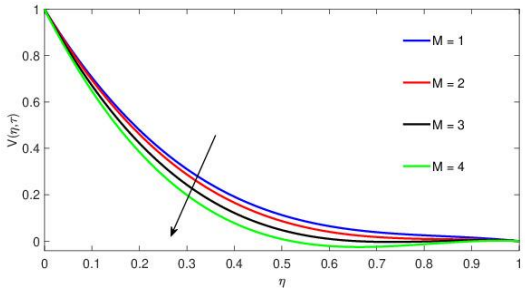

Fig 3: Impacts of M on $V(\eta,\tau)$

Figure 4 elucidates the influence of suction $(S > 0)$ on the velocity fields. Graphically, it's observed that the velocity field drops as the values of the suction parameter rises. Physically, rising suction implies that removal of the fluid from the flow system or the fluid flow system gets altered to slow down which can be evident through graph that decrease the velocity boundary layer thickness and thus velocity profiles drop.

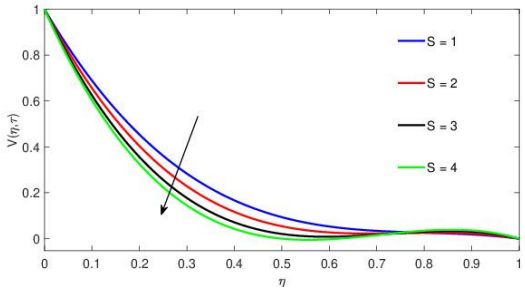

Fig 4: Impacts of S on $V(\eta,\tau)$

Figure 5 displays the velocity field profiles versus η for various values of viscosity fluid parameter. Graphically, it is interesting to seen that the velocity fields recedes with larger values of viscosity parameter. Physically, for higher values of fluid viscosity parameter decline the momentum boundary layer thickness due to the larger temperature difference between the surface of the flat plate and an ambient fluid.

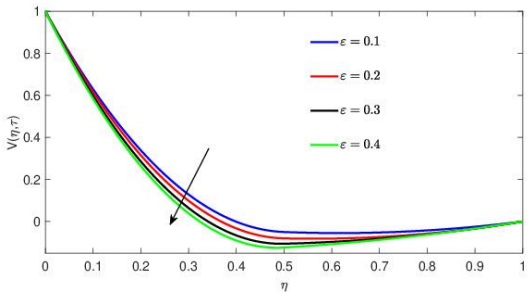

Fig 5: Impacts of ε on $V(\eta,\tau)$

Figure 6 depicts the impacts of Soret number (Sr) on the concentration of the fluid. Graphically, it's observed that a rise in the Soret number results to an increase of the field concentration.As expected, physically, rising the values of Soret number leads to a rise in the solutal boundary layer due to an increase in the field concentration in the fluid flow and thus increase the concentration boundary layer thickness which can be evident from through graph that the concentration profiles rises.

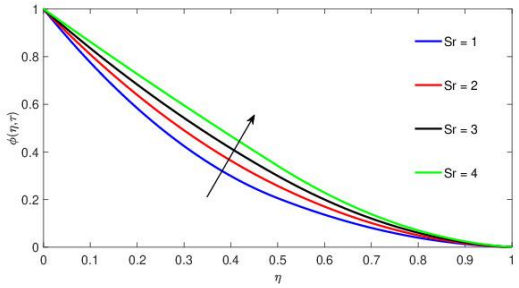

Fig 6: Impacts of Sr on $\phi(\eta,\tau)$

The influence of Schmidt number on the fluid concentration is display in Figure 7. It's noted that the fluid concentration drops as the results of an increment of Schmidt number. As expected, physically, rising the Schmidt number cause a decrease of molecular or diffusion on the flow and results to decrease in the solutal boundary layer thickness and thus decline in the field concentration profiles.

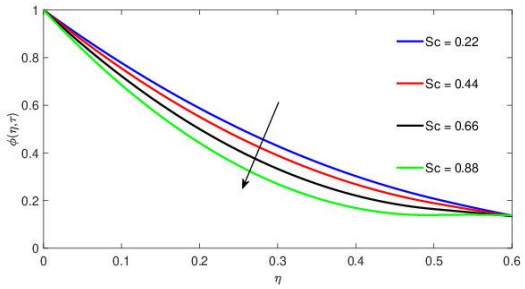

Fig 7: Impacts of Sc on $\phi(\eta,\tau)$

Figure 8 displays the impacts of suction parameter $(S > 0)$ on the fluid concentration. Graphically, it's observed that a rise suction parameter leads to declined in species concentration profiles. Physically, rising the suction results to the flow gets altered to slow down which decline the species boundary layer thickness and thus concentration profiles drops.

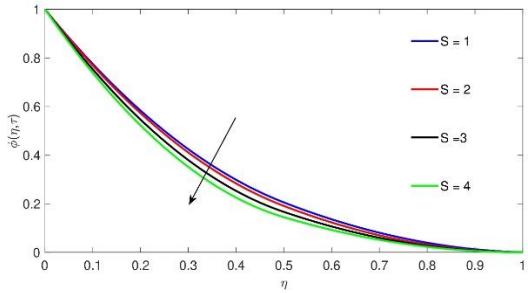

Fig 8: Impacts of S on $\phi(\eta,\tau)$

Figure 9 depicts the effects of suction parameter $(S > 0)$ on the induced magnetic field. It's observed from the graph that a rise in suction parameter causes a decline in the induced magnetic field profiles. As expected. physically, increasing suction in the flow cause the the flow gets altered to slow down which results to recedes in the interaction of the fluid and magnetic field in the flow and thus recedes induced magnetic field profiles.

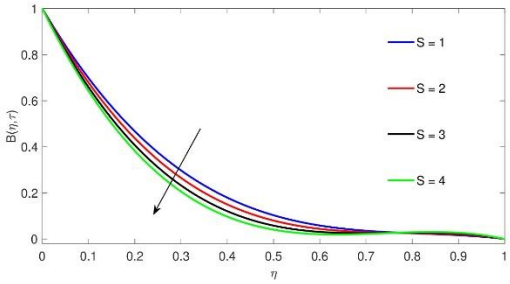

Fig 9: Impacts of S on $B(\eta,\tau)$

Figure 10 depicts the induced magnetic field profiles against η for different values of magnetic Prandtl number (Prm). It's noted form the graph that induced magnetic profiles rises with higher values of (Prm). Physically, rising the values of (Prm) results to a decline magnetic diffusivity and causes interaction between the fluid and magnetic field to increase and thus induced magnetic field profiles rises.

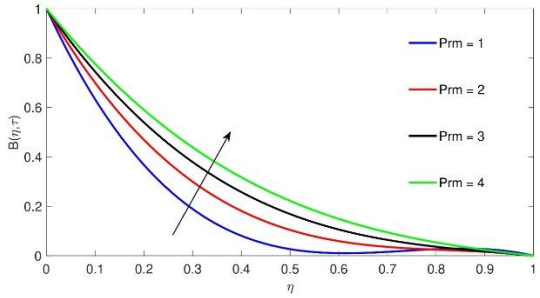

Fig 10: Impacts of Prm on $B(\eta,\tau)$

Figure 11 shows the influence of heat source parameter (Q) on the fluid temperature. Graphically, it's noted that larger values of (Q) causes a rises in the fluid's temperature. Physically, rising heat source causes the fluid to generate no heat in the fluid which results to grows in the thermal boundary layer thickness and thus thermal field profiles rises

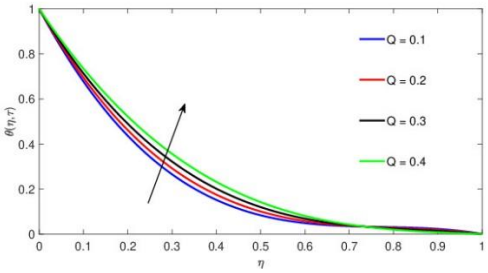

Fig 11: Impacts of Q on $\theta(\eta,\tau)$

Figure 12 presents the impacts of Dufour number (Du) on on the fluid's temperature. Graphically, it's observed that the fluid temperature profiles rises rapidly as the Dufour number rises.

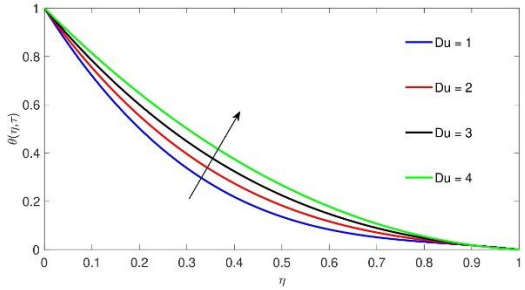

Fig 12: Impacts of Du on $\theta(\eta,\tau)$

Figure 13 demonstrates the influence of Eckert number (Er) on the fluid temperature profiles. Graphically, it's noted that a rise in the Eckert number (Ec) causes a rises in the fluid's temperature. Physically, as Eckert number rises causes a reduction of fluid's enthalpy in the flow system and thus thermal energy in the flow is converted into kinetic energy which rises of the thermal boundary layer thickness.

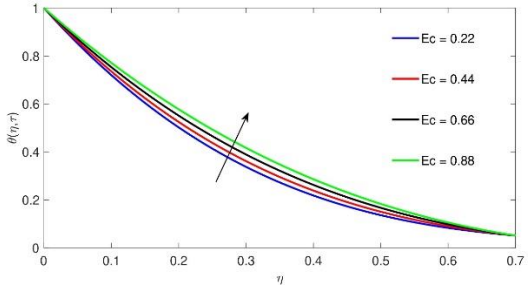

Fig 13: Impacts of Ec on $\theta(\eta,\tau)$

Figure 14 depicts the impacts of thermal radiation parameter (Rd) on the thermal field profiles. Graphically, it' noted that a rise in the thermal radiation parameter causes a growth in the fluid's temperature. As expected, rising of thermal radiation results to the combined impacts of heat to thermal emission transportation rates. Therefore increment of thermal radiation enhances the thermal boundary layer thickness and thus grows the fluid temperature profiles.

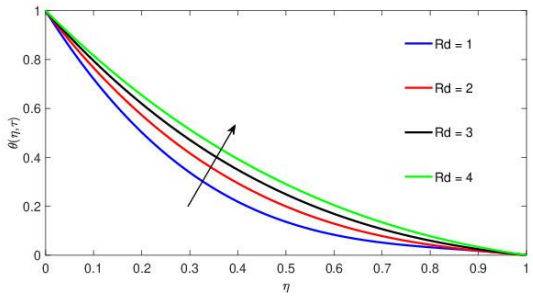

Fig 14: Impacts of Rd on $\theta(\eta,\tau)$

Figure 15 displays the impacts of suction variable $(S > 0)$ on the temperature profiles. From the graph, it's observed that enhancement of suction variable results to a decline in the thermal field.

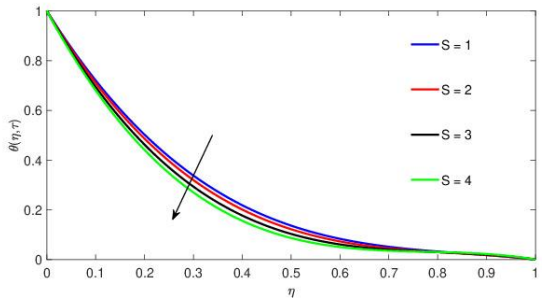

Fig 15: Impacts of S on $\theta(\eta,\tau)$

Figure 16 presents the impacts of Prandtl number (Pr) on the thermal field. Graphically, it's that enhancement of Prandtl number causes recedes in the thermal field. As expected, rising the Prandtl number leads to reduction of fluid's thermal diffusivity and increases viscous drag in the fluid which results to recedes in the thermal field.

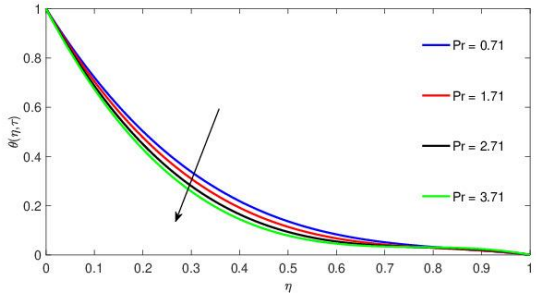

Fig 16: Impacts of Pr on $\theta(\eta,\tau)$

The thermal field profiles against η is shown in Figure 17. it's revealed that the thermal fields grows with large values of fluid viscosity parameter. Physically, rising the values of fluid viscosity parameter grows significantly the thermal boundary layer and thus thermal field profiles rises.

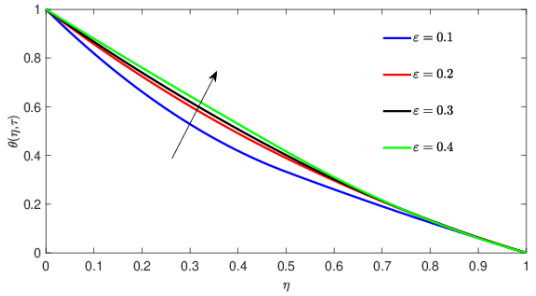

Fig 17: Impacts of ε on $\theta(\eta,\tau)$

Figure 20 depicts the impacts of Brinkman number (Br) on on the entropy profiles. Graphically, it's noted that an enhance of Brinkman number causes a viscosity in the fluid and thus results to an increase in the entropy profiles.

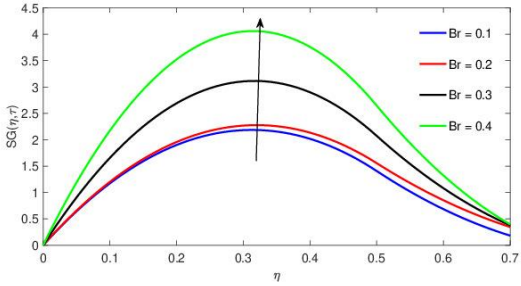

Fig 18: Impacts of Br on $SG(\eta,\tau)$

Figure 19 demonstrates the influence of magnetic Prandtl number (Prm) on the entropy profiles. Graphically, it's observed that a rise in the magnetic Prandtl number causes an increase in the entropy profiles. Physically, Increasing magnetic Prandtl number causes an increase of Lorentz force which leads to an improvement of entropy generation.

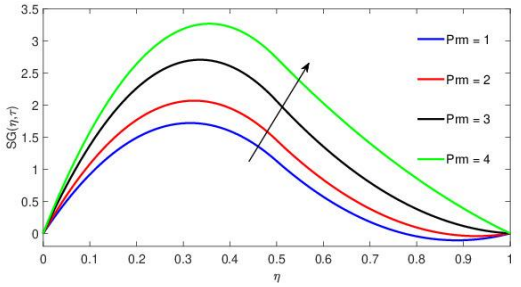

Fig 19: Impacts of Prm on $SG(\eta,\tau)$

Figure 20 presents the impacts of thermal radiation paramater on the entropy profiles. Graphically, it has been noted that enhance of thermal radiation causes an improvement of entropy profiles.

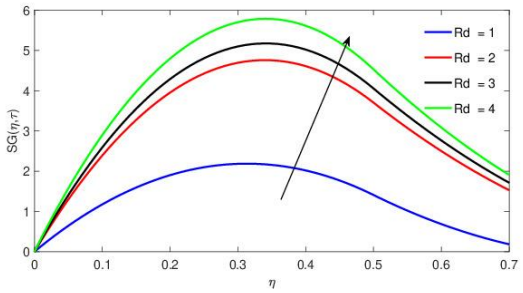

Fig 20: Impacts of Rd on $SG(\eta,\tau)$

Figure 21 elucidates the impacts of Brinkman number on the Bejan number. Graphically, it's observed that higher values of Brinkman number recede the Bejan number.

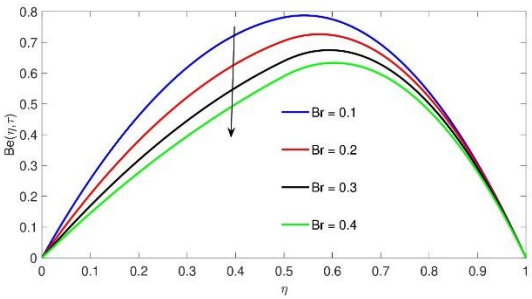

Fig 21: Impacts of Br on Be

Figure 22 demonstrates the impacts of thermal radiation parameter on the Bejan number. Graphically, it's observed the decline of Bejan number with lager values of magnetic Prandtl number.

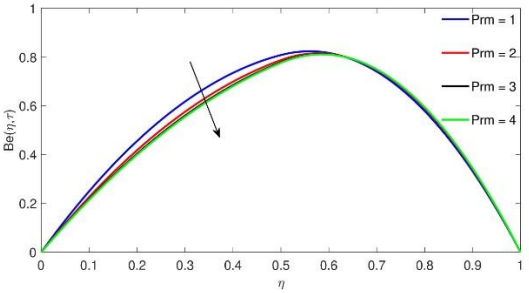

Fig 22: Impacts of Prm on Be

Figure 23 shows the impacts of source parameter on the Bejan number. Graphically, it's observed that lager values of source parameter signifies the Bejan number.

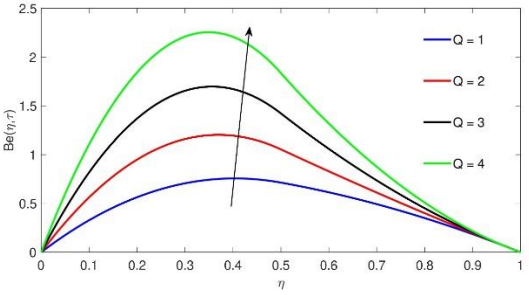

Fig 23: Impacts of Q on Be

Figure 24 depicts the impacts of thermal radiation parameter on the Bejan number. Graphically, it's observed

that lager values of thermal radiation parameter amplifies the Bejan number.

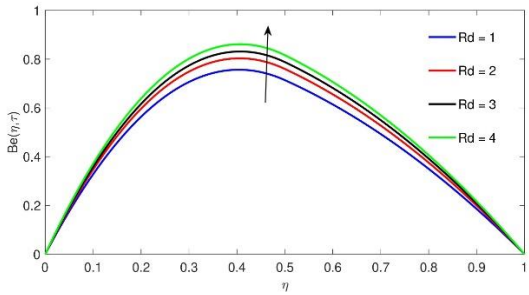

Fig 24: Impacts of Rd on Be

Figure 25 elucidates the impacts of thermal radiation parameter on the Bejan number. Graphically, it's observed the decline of Bejan number with rising the values of Soret number.

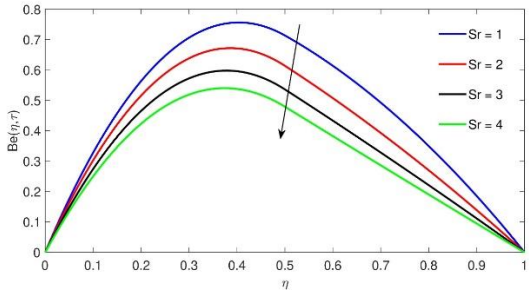

Fig 25: Impacts of Sr on Be

Figure 26 demonstrates the impacts of Dufour number on the Bejan number. Graphically, it's observed that rising the values of Dufour number recede the Bejan number.

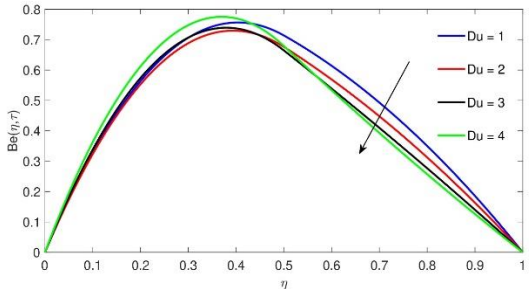

Fig 26: Impacts of Du on Be

Figure 27, shows the numerical validation of the present results with the previous results from the literature. The results of the present study agree with the results of [?], which show good agreement and the numerical code is excellent under limited case when $\varepsilon = 0, \beta = \alpha = 0$ and absence of induced magnetic field.

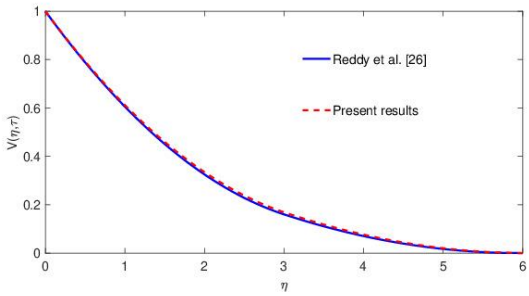

Fig 27: Validation of numerical results of the present study and the results obtained by [?]

CONCLUDING REMARKS

This paper scrutinizes the entropy generation of the radiative heat and mass transfer characteristics of time dependent flow with variable fluid viscosity, induced magnetic field, Dufour and Soret impacts using Caputo Fabrizio fractal fractional order derivative operators. An approximate solution for the system of non-linear PDEs are solved numerically using finite difference method and the computational outcomes of the flow fields against the embedded parameters are investigated and represented graphically. The major outcomes of the current analysis are summarized as follows:-

(i) The fractal fractional parameters enhance the velocity field profiles. Also, it's seen that fractal fractional parameter β has larger memory effect compared to fractional order parameter α .

(ii) The rising the values of fluid variable viscosity parameter ε , magnetic parameter M and suction parameter S results to recedes of the velocity field profiles.

(iii) The progressively increment of Soret number Sr rises the concentration field whereas decline in the concentration field profiles is noted when suction parameter s and Schmidt number progressively incremented.

(iv) Higher values of magnetic Prandtl number Prm rises the induced magnetic field profiles whereas decreases as the suction parameter S rises.

(v) Thermal field is incremented with rising the values of fluid variable viscosity parameter ε , heat source parameter Q, Dufour number Du, Eckert number Ec and thermal radiation parameter Rd, but it's decrease against the values of suction parameter S and Prandtl number Pr

(vi) Entropy generation rate is incremented with rising the values of Brinkman number Br, magnetic Prandtl number Prm and approximation of thermal radiation Rd

(vii) Bejan number recedes with rising the values of Brinkman number Br and magnetic Prandtl number Prm, but it's increases against the values of heat source parameter S and thermal radiation parameter Rd

The findings are useful for researching on how to restrict energy losses during energy production in the form of heat dissipation, especially when dealing with heat transfer issues.

Declaration of competing interest

The authors declare that they have no known competing financial interests or personal relationships that could have appeared to influence the work reported in this paper.

Data Availability

The data used to support the findings of this study are included within the article.

REFERENCES

[1] S. Li, K. Raghunath, A. Alfaleh, F. Ali, A. Zaib,

M. I. Khan, S. M. ElDin, V. Puneeth,Effects of activation energy and chemical reaction on unsteady mhd dissipative darcy– forchheimer squeezed flow of casson fluid over horizontal channel, Scientific Reports 13 (2023) 2666.

[2] Y.-M. Chu, S. Jakeer, S. Reddy, M. L. Rupa, Y. Trabelsi, M. I. Khan, H. A. Hejazi, B. M. Makhdoum, S. M. Eldin, Double diffusion effect on the bio-convective magnetized flowof tangent hyperbolic liquid by a stretched nano-material with arrhenius catalysts, Case Studies in Thermal Engineering 44 (2023) 102838.

[3] Z. Liu, S. Li, T. Sadaf, S. U. Khan, F. Alzahrani, M. I. Khan, S. M. Eldin, Numerical bio-convective assessment for rate type nanofluid influenced by nield thermal constraints and distinct slip features, Case Studies in Thermal Engineering 44 (2023) 102821.

[4] S. Li, F. Ali, A. Zaib, K. Loganathan, S. M. Eldin, M. Ijaz Khan, Bioconvection effect inthe carreau nanofluid with cattaneo–christov heat flux using stagnation point flow in the entropy generation: Micromachines level study, Open Physics 21 (2023) 20220228.

[5] Z. Hussain, W. A. Khan, T. Muhammad, H. A. Alghamdi, M. Ali, M. Waqas, Dynamics of gyrotactic microorganisms for chemically reactive magnetized 3d sutterby nanofluid flow comprising non-uniform heat sink-source aspects, Journal of Magnetism and Magnetic Materials 578 (2023) 170798.

[6] I. Hussain, W. Khan, M. Tabrez, S. Elattar, M. I. Khan, Impact of ferromagnetic nanopar- ticles on convectively heated radiative flow of williamson nanofluid, Journal of the Indian Chemical Society 100 (2023) 100915.

[7] S. Zafar, A. Alfaleh, A. Zaib, F. Ali, M. Faizan, A. M. Abed, S. Elattar, M. I. Khan, Simulation of prandtl nanofluid in the mixed convective flow of activation energy with gyrotactic microorganisms: Numerical outlook features of micro-machines, Micromachines14 (2023) 559.

[8] M. Waqas, M. S. Kausar, O. A. Bég, S. Kuharat, W. Khan, S. S. Abdullaev, B. M. Fadhl, Numerical study of dissipative sw/mwcnt-nanofluid coating flow from a stretching wallto a porous medium with shape factor effects, International Journal of Hydrogen Energy (2023).

[9] N. Rathore, N. Sandeep, Solar thermal energy performance on mono/trihybrid nanofluid flow through the evacuated thermal collector tube, International Journal of Hydrogen Energy (2023).

[10] Y.-M. Chu, F. Alzahrani, O. Mopuri, C. Ganteda, M. I. Khan, S. U. Khan, S. M. Eldin,et al., Thermal impact of hybrid nanofluid due to inclined oscillatory porous surface with thermo-diffusion features, Case Studies in Thermal Engineering 42 (2023) 102695.

[11] N. Abbas, W. Shatanawi, K. Abodayeh, T. A. Shatnawi, Comparative analysis of un- steady flow of induced mhd radiative sutterby fluid flow at nonlinear stretching cylin- der/sheet: Variable thermal conductivity, Alexandria Engineering Journal 72 (2023) 451– 461.

[12] F. Wang, W. Jamshed, R. W. Ibrahim, N. S. E. Abdalla, A. Abd-Elmonem, S. M. Hus-sain, et al., Solar radiative and chemical reactive influences on electromagnetic maxwell nanofluid flow in buongiorno model, Journal of Magnetism and Magnetic Materials 576 (2023) 170748.

[13] M. S. Babu, G. R. Sankar, V. R. Velpula, Y.-M. Chu, M. I. Khan, C. Raju, H. A. Hejazi, B. M. Makhdoum, S. M. Eldin, Chemically reactive flow of viscous thermophoretic fluid over wedge with variable thermal conductivity and viscosity, Case Studies in Thermal Engineering 45 (2023) 102924.

[14] N. B. Kheder, S. Rehman, S. Alqahtani, S. Alshehery, et al., Comparative study of entropy distribution for generalized fluid between an inclined channel in the perspective of classical and non-fourier's law, Engineering Science and Technology, an International Journal 45 (2023) 101471.

[15] T. Sajid, M. K. Al Mesfer, W. Jamshed, M. R. Eid, M. Danish, K. Irshad, R. W. Ibrahim, S. Batool, S. M. El Din, G. C. Altamirano, Endo/exothermic chemical processes influences of tri-hybridity nanofluids flowing over wedge with convective boundary constraints and activation energy, Results in Physics (2023) 106676.

[16] M. Nazeer, M. W. Nazir, N. Ali, T. Javed, S. A. Abdelmohsen, M. I. Khan, Momentum and thermal transport analysis in mhd nanofluid through the thermally heated square conduit: Finite element method, Journal of Magnetism and Magnetic Materials (2023) 170954.

[17] M. ur Rahman, F. Haq, P. C. Darab, M. Sallah, S. A. Abdelmohsen, B. M. Fadhl, B. M. Makhdoum, Mixed convection and activation energy impacts on mhd bioconvective flow of nanofluid with irreversibility assessment, Heliyon 9 (2023).

[18] H. Maaitah, A. N. Olimat, O. Quran, H. M. Duwairi, Viscous dissipation analysis of williamson fluid over a horizontal saturated porous plate at constant wall temperature, International Journal of Thermofluids 19 (2023) 100361.

[19] R. Kodi, R. R. Vaddemani, M. I. Khan, S. S. Abdullaev, A. Boudjemline, M. Boujelbene, Y. Bouazzi, et al., Unsteady magneto-hydro-dynamics flow of jeffrey fluid through porous media with thermal radiation, hall current and soret effects, Journal of Magnetism and Magnetic Materials (2023) 171033.

[20] F. Ali, A. Zaib, B. S. Abdullaeva, R. Altuijri, M. I. Khan, Darcy forchheimer flow ofterny hybrid nanofluid flow through a blood circulation respiratory system, Colloid andPolymer Science (2023) 1–13.

[21] R. Mahesh, A. Vishalakshi, U. Mahabaleshwar, F. Sofos, Impact of an inclined magnetic field on couple stress fluid flow over a stretching surface with effect of stefan blowing, radiation and chemical reaction, Journal of Magnetism and Magnetic Materials (2023) 170953.

[22] C. Sowmiya, B. R. Kumar, Mhd maxwell nanofluid flow over a stretching cylinder in porous media with microorganisms and activation energy, Journal of Magnetism and Magnetic Materials (2023) 171032.

[23] B. K. Sharma, C. Kumawat, U. Khanduri, K. S. Mekheimer, Numerical investigation of the entropy generation analysis for radiative mhd power-law fluid flow of blood througha curved artery with hall effect, Waves in Random and Complex Media (2023) 1–38.

[24] M. Basit, M. Tahir, A. Riasat, S. Khan, M. Imran, A. Akgül, Numerical simulation of bioconvective casson nanofluid through an exponentially permeable stretching surface, International Journal of Modern Physics B (2023) 2450128.

[25] A. Hobiny, M. Tabrez, W. Khan, I. Hussain, Numerical analysis of ferromagnetic carreaufluid flow comprising viscos dissipation aspects, Modern Physics Letters B (2023) 2341003.

[26] Y. D. Reddy, D. Ramya, L. A. Babu, Effect of thermal radiation on mhd boundary layer flow of nanofluid and heat transfer over a non-linearly stretching sheet with transpiration,Journal of Nanofluids 5 (2016) 889–897.

[27] M. M. Bhatti, T. Abbas, M. Rashidi, Numerical study of entropy generation with non-linear thermal radiation on magnetohydrodynamics non-newtonian nanofluid through a porous shrinking sheet, Journal of Magnetics 21 (2016) 468–475.

[28] P. Sudarsana Reddy, P. Sreedevi, Entropy generation and heat transfer analysis of mag- netic hybrid nanofluid inside a square cavity with thermal radiation, The European Physical Journal Plus 136 (2021) 1–33.

[29] A. Sahoo, R. Nandkeolyar, Entropy generation and dissipative heat transfer analysis of mixed convective hydromagnetic flow of a casson nanofluid with thermal radiation and hall current, Scientific Reports 11 (2021) 3926.

[30] A. Lopez, G. Ibanez, J. Pantoja, J. Moreira, O. Lastres, Entropy generation analysis of mhd nanofluid flow in a porous vertical microchannel with nonlinear thermal radiation, slip flow and convective-radiative boundary conditions, International Journal of Heat and Mass Transfer 107 (2017) 982–994.

[31] P. B. A. Reddy, Biomedical aspects of entropy generation on electromagnetohydrody- namic blood flow of hybrid nanofluid with nonlinear thermal radiation and non-uniform heat source/sink, The European Physical Journal Plus 135 (2020) 1–30.

[32] M. I. Khan, S. Qayyum, T. Hayat, M. Waqas, M. I. Khan, A. Alsaedi, Entropy genera- tion minimization and binary chemical reaction with arrhenius activation energy in mhd radiative flow of nanomaterial, Journal of Molecular Liquids 259 (2018) 274–283.

[33] S. Salawu, H. Ogunseye, Entropy generation of a radiative hydromagnetic powell-eyring chemical reaction nanofluid with variable conductivity and electric field loading, Resultsin Engineering 5 (2020) 100072.

[34] H. Ullah, T. Hayat, S. Ahmad, M. S. Alhodaly, Entropy generation and heat transfer analysis in power-law fluid flow: Finite difference method, International Communications in Heat and Mass Transfer 122 (2021) 105111.

[35] R. Muhammad, M. I. Khan, N. B. Khan, M. Jameel, Magnetohydrodynamics (mhd) radiated nanomaterial viscous material flow by a curved surface with second order slipand entropy generation, Computer methods and programs in biomedicine 189 (2020) 105294.

[36] Z. Shah, P. Kumam, W. Deebani, Radiative mhd casson nanofluid flow with activation energy and chemical reaction over past nonlinearly stretching surface through entropy generation, Scientific reports 10 (2020) 4402.

[37] M. I. Khan, T. Hayat, M. I. Khan, M. Waqas, A. Alsaedi, Numerical simulation of hy- dromagnetic mixed convective radiative slip flow with variable fluid properties: a math- ematical model for entropy generation, Journal of Physics and Chemistry of Solids 125(2019) 153–164.

[38] S. A. Khan, T. Hayat, M. I. Khan, A. Alsaedi, Salient features of dufour and soreteffect in radiative mhd flow of viscous fluid by a rotating cone with entropy generation, International Journal of Hydrogen Energy 45 (2020) 14552–14564.

[39] S. A. Khan, T. Hayat, A. Alsaedi, M. Alhodaly, Thermal analysis for radiative flow of darcy–forchheimer nanomaterials subject to entropy generation, Journal of Computational Design and Engineering 9 (2022) 1756–1764.

[40] T. Hayat, S. A. Khan, S. Momani, Finite difference analysis for entropy optimized flow of casson fluid with thermo diffusion and diffusion-thermo effects, International Journal of Hydrogen Energy 47 (2022) 8048–8059.

[41] A. Subramanyam Reddy, T. Thamizharasan, et al., Pulsatile flow of jeffrey hybrid nanofluid in a vertical channel with entropy generation, Indian Journal of Chemical Technology (IJCT) 30 (2023) 534–546.

[42] P. K. Dadheech, P. Agrawal, A. Sharma, A. Dadheech, Q. Al-Mdallal, S. D. Purohit, Entropy analysis for radiative inclined mhd slip flow with heat source in porous medium for two different fluids, Case Studies in Thermal Engineering 28 (2021) 101491.

[43] S. A. Khan, T. Hayat, A. Alsaedi, Entropy generation in chemically reactive flow of reiner-rivlin liquid conveying tiny particles considering thermal radiation, Alexandria Engineering Journal 66 (2023) 257–268.

[44] S. Li, M. I. Khan, F. Alzahrani, S. M. Eldin, Heat and mass transport analysis in radiative time dependent flow in the presence of ohmic heating and chemical reaction, viscous dissipation: An entropy modeling, Case Studies in Thermal Engineering 42 (2023) 102722.

[45] S. Li, M. I. Khan, A. B. Alruqi, S. U. Khan, S. S. Abdullaev, B. M. Fadhl, B. M. Makhdoum, Entropy optimized flow of sutterby nanomaterial subject to porous medium: Buongiorno nanofluid model, Heliyon (2023).

[46] S. M. Hussain, U. Khan, A. Zaib, A. Ishak, I. E. Sarris, Numerical computation of mixed convective entropy optimized in darcy-forchheimer flow of cross nanofluids through a vertical flat plate with irregular heat source/sink, Tribology International (2023) 108757.

[47] S. Murtaza, P. Kumam, Z. Ahmad, K. Sitthithakerngkiet, I. E. Ali, Finite difference simulation of fractal-fractional model of electro-osmotic flow of casson fluid in a micro channel, IEEE Access 10 (2022) 26681–26692.

[48] N. Ahmed, Mhd radiating flow with thermal diffusion, and diffusion-thermo, in: Thermal and Solutal Convection in Some Hydromagnetic Flows, Springer, 2023, pp. 175–198.

[49] G. C. Mouli, K. Gangadhar, B. H. S. Raju, On spectral relaxation approach for soret and dufour effects on sutterby fluid past a stretching sheet, International Journal of Ambient Energy 43 (2022) 500–507.

[50] B. Falodun, A. Ayoade, O. Odetunde, Positive and negative soret and dufour mechanism on unsteady heat and mass transfer flow in the presence of viscous dissipation, thermal and mass buoyancy, Australian Journal of Mechanical Engineering 21 (2023) 965–978.

[51] K. K. Asogwa, M. Alsulami, B. Prasannakumara, T. Muhammad, Double diffusive con- vection and cross diffusion effects on casson fluid over a lorentz force driven riga plate ina porous medium with heat sink: An analytical approach, International Communicationsin Heat and Mass Transfer 131 (2022) 105761.

[52] D. K. Prasad, G. K. Chaitanya, R. S. Raju, Double diffusive effects on mixed convection casson fluid flow past a wavy inclined plate in presence of darcian porous medium, Results in Engineering 3 (2019) 100019.

[53] S. Akram, M. Athar, K. Saeed, A. Razia, Theoretical analysis of partial slip on double- diffusion convection of eyring-powell nanofluids under the effects of peristaltic propulsion and inclined magnetic field, Journal of Magnetism and Magnetic Materials 569 (2023) 170445.

[54] S. Negi, S. K. Rawat, M. Kumar, Cattaneo–christov double-diffusion model with stefan blowing effect on copper–water nanofluid flow over a stretching surface, Heat Transfer 50(2021) 5485–5515.

[55] P. Mondal, T. Mahapatra, MHD double-diffusive mixed convection and entropy generation of nanofluid in a trapezoidal cavity, International Journal of Mechanical Sciences 208 (2021) 106665.

[56] N. J. Noon, S. Haddad, Stability analysis for rotating double-diffusive convection in the presence of variable gravity and reaction effects: darcy model, Special Topics & Reviews in Porous Media: An International Journal 13 (2022).

[57] A. Bouachir, M. Mamou, R. Rebhi, S. Benissaad, Linear and nonlinear stability analyses of double-diffusive convection in a vertical brinkman porous enclosure under soret and dufour effects, Fluids 6 (2021) 292.

[58] N. Vijay, K. Sharma, Magnetohydrodynamic hybrid nanofluid flow over a decelerating rotating disk with soret and dufour effects, Multidiscipline Modeling in Materials and Structures 19 (2023) 253–276.

[59] N. K. Mishra, M. Sharma, B. Sharma, U. Khanduri, Soret and dufour effects on mhd nanofluid flow of blood through a stenosed artery with variable viscosity, International Journal of Modern Physics B (2023) 2350266.

[60] M. Ramzan, N. Shahmir, H. A. S. Ghazwani, Y. Elmasry, S. Kadry, A numerical study of nanofluid flow over a curved surface with cattaneo–christov heat flux influenced by induced magnetic field, Numerical Heat Transfer, Part A: Applications 83 (2023) 197–212.

[61] J. Mng'ang'a, M. Kinyanjui, E. R. Onyango, Hydromagnetic surface driven flow between two parallel vertical plates in the presence of chemical reaction and induced magnetic field, Global Journal of Pure and Applied Mathematics 18 (2022) 583–612.

[62] S. Dolui, B. Bhaumik, S. De, Combined effect of induced magnetic field and thermal radiation on ternary hybrid nanofluid flow through an inclined catheterized artery with multiple stenosis, Chemical Physics Letters 811 (2023) 140209.

[63] U. Khan, A. Zaib, A. Ishak, I. Waini, I. Pop, S. Elattar, A. M. Abed, Stagnation point flow of a water-based graphene-oxide over a stretching/shrinking sheet under an induced magnetic field with homogeneous-heterogeneous chemical reaction, Journal of Magnetism and Magnetic Materials 565 (2023) 170287.

[64] S. Akram, M. Athar, K. Saeed, A. Razia, T. Muhammad, H. A. Alghamdi, Mathematical simulation of double diffusion convection on peristaltic pumping of ellis nanofluid due to induced magnetic field in a non-uniform channel: Applications of magnetic nanoparticles in biomedical engineering, Journal of Magnetism and Magnetic Materials 569 (2023) 170408.

[65] J. Mng'ang'a, Effects of chemical reaction and joule heating on mhd generalized couette flow between two parallel vertical porous plates with induced magnetic field and newtonian heating/cooling, International Journal of Mathematics and Mathematical Sciences 2023 (2023).

[66] S. Akram, M. Athar, K. Saeed, A. Razia, T. Muhammad, A. Hussain, Hybrid double- diffusivity convection and induced magnetic field effects on peristaltic waves of oldroyd 4-constant nanofluids in non-uniform channel, Alexandria Engineering Journal 65 (2023) 785–796.

[67] S. Akram, A. Razia, M. Y. Umair, T. Abdulrazzaq, R. Z. Homod, Double-diffusive convection on peristaltic flow of hyperbolic tangent nanofluid in non-uniform channel with induced magnetic field, Mathematical Methods in the Applied Sciences 46 (2023) 11550–11567.

[68] J. Mng'ang'a, Effects of ohmic heating, induced magnetic field and newtonian heat- ing on magnetohydrodynamic generalized couette flow of jeffrey nanofluid between two parallel horizontal plates with convective cooling, International Journal of Thermoflu- ids 20 (2023) 100402. URL: https://www.sciencedirect.com/science/article/pii/S2666202723001192. doi:.

[69] J. K. Singh, S. Kolasani, Hanumantha, G. S. Seth, Scrutiny of induced magnetic fieldand hall current impacts on transient hydromagnetic nanofluid flow within two vertical alternative magnetized surfaces, Proceedings of the Institution of Mechanical Engineers, Part E: Journal of Process Mechanical Engineering 237 (2023) 1595–1606.

[70] R. Mahato, M. Das, S. Sen, R. Nandkeolyar, Hydromagnetic mixed convection unsteady radiative casson fluid flow towards a stagnation-point with chemical reaction, induced magnetic field, soret effect, and convective boundary conditions, Heat Transfer 52 (2023) 1142–1160.

[71] M. M. Alam, M. R. Islam, F. Rahman, Study heat and mass transfer by mixed convection flow from a vertical porous plate with induced magnetic field, constant heat and mass fluxes, Science & technology asia (2008) 1–13.

[72] S. Poddar, M. M. Islam, J. Ferdouse, M. M. Alam, Characteristical analysis of mhd heat and mass transfer dissipative and radiating fluid flow with magnetic field induction and suction, SN Applied Sciences 3 (2021) 1–17.

[73] O. D. Makinde, O. Franks, On mhd unsteady reactive couette flow with heat transferand variable properties, Central European Journal of Engineering 4 (2014) 54–63.

[74] J. Mng'ang'a, E. R. Onyango and K.J. Chillingo. "Joule heating and induced magnetic field on magnetohydrodynamic generalised Couette flow of Jeffrey fluid in an inclined channel with Soret and Dufour effects." *International Journal of Ambient Energy* 45.1 (2024): 2305328.

